Tunning thermoelectric properties of $Ca_{0.9}Gd_{0.1}MnO_3$ by laser processing

N.M. Ferreira[1], A.R. Sarabando[2], M.C. Ferro[2], M. A. Madre[3], O.J. Dura[4], A. Sotelo[3],

[1]I3N, Physics Department, University of Aveiro, 3810-193 Aveiro, Portugal

[2] CICECO - Aveiro Institute of Materials, Department of Materials and Ceramic Engineering, University of Aveiro, 3810-193 Aveiro, Portugal

[3] ICMA, CSIC-Universidad de Zaragoza, Zaragoza, Spain

[4] Applied Physics Department, University of Castilla-La Mancha, Spain

*corresponding author: nmferreira@ua.pt

Abstract

Donor-doped $CaMnO_3$ is an n-type semiconductor with perovskite structure, being considered as a potential n-type leg in thermoelectric modules. This oxide presents stability at high temperatures and allows tuning the relevant electrical and thermal transport properties through doping. In this work, $Ca_{0.9}Gd_{0.1}MnO_3$ precursors have been prepared to produce fibres through the laser floating zone technique using different pulling rates. However, as-grown fibres did not present thermoelectric properties due to the presence of high amounts of secondary phases, leading to very high electrical resistivity values. The results have highlighted the importance of annealing procedures to reduce electrical resistivity, due to the decrease of secondary phases amount, and producing promising thermoelectric performances. The annealed samples present higher ZT values when the growth rate is decreased, reaching around 0.22 for the lowest growth rate, which is very close to the best values reported in the literature for these materials. Moreover, this procedure possesses an additional advantage considering that these samples can be directly used as n-type legs in thermoelectric modules for high-temperature applications However, further studies should be made to determine the optimal amount of dopant.

Keywords:

Laser Floating Zone, Calcium manganite, Oxides; Thermoelectrics, Electrical properties, ceramics

Introduction

The capacity of converting waste heat into electric energy by thermoelectric (TE) materials, with no needs of moving parts and without producing carbon dioxide gas, toxic substances, or other emissions, are gaining scientific and industrial interest. With this purpose, different materials are proposed to be used in thermoelectric devices. Transition oxides-based ceramics are one of the most promising, due to their high thermal and chemical stability when working under oxidizing atmospheres, at high temperatures [1]. Among the n-type semiconductor oxides, $CaMnO_3$ is regarded as one of the most suitable ones [2-8]; however, this compound possesses limited TE performances due to its low carrier concentration [1 - 6]. Consequently, many studies have been carried out to improve its thermoelectric properties using dopants and different preparation techniques [2-6,9-11]. These studies are essentially focused on the improvement of electrical conductivity, without drastically affecting Seebeck coefficient or thermal conductivity. On the other hand, doping processes have already proved to increase electrical conductivity and, simultaneously, reduce thermal conductivity [4,11-13]. This is of the main importance, as the thermoelectric performances are evaluated using the dimensionless figure-of-merit, ZT, which combines Seebeck coefficient (S), absolute temperature (T), electrical resistivity (ρ), and thermal conductivity (κ), and it is defined as $S^2T/\rho\kappa$ [1,14], where S^2/ρ is called power factor, PF.

Several works studied $(Ca,Gd)MnO_{3-\delta}$ polycrystalline samples with high thermoelectric properties [4,5, and references therein]. The results of electrical resistivity have been well correlated to the Mn valence and oxygen deficiency. Moreover, they have verified that gadolinium doping on the calcium site reduces the electrical resistivity and thermal conductivity values [4,5].

On the other hand, it is well known that preparation routes present a significant impact on the thermoelectric performance. Microstructural tuning is quite effective for decreasing electrical resistivity and thermal conductivity while increasing, or maintaining practically constant, Seebeck coefficient [3,15-17]. In the present work, $Ca_{0.9}Gd_{0.1}MnO_3$ samples were grown through the laser

floating zone method with different pulling rates to understand the effect of the solidification rate on their thermoelectric performances.

Eperimental procedure

The raw starting material, with $Ca_{0.9}Gd_{0.1}MnO_3$ (mol%) composition, has been prepared using $CaCO_3$ (Panreac, 99,5%), MnO (Panreac, 99%) and Gd_2O_3 (Aldrich, 99,9 %) commercial powders. They were weighed in stoichiometric proportions and ball-milled at 300 rpm for 30 minutes. PVA (PolyVinyl Alcohol) was added to the obtained mixture to allow the production of cylindrical rods by cold extrusion. These extruded rods, after drying, presented ~ 3 mm diameter, being used as precursors in a laser floating zone system, equipped with an continuous CO_2 laser (80 Watt, λ = 10.6 μm), described elsewhere [11]. The rods were then directionally grown between 10 and 200 mm h^{-1} solidification rates, and maintaining the other growth parameters unchanged from the optimal found in previous works [11,12]: Seed was rotated at 5 rpm to maintain the cylindrical geometry, while feed was rotated at 15 rpm in the opposite direction to compositionally homogeneize the molten zone. After the growth process, dimensionally homogeneous fibres with ~ 2.5 mm diameter, were obtained. On the other hand, as previously mentioned, these as-grown materials are characterized by a large amount of secondary phases due to their incongruent melting [12], leading to relatively low thermoelectric performances. As a consequence, it is necessary to produce the thermoelectric phase from the secondary ones. It can be performed by annealing at 1300 ºC during 10h under air, drastically increasing thermoelectric properties, as reported in similar works [3,5,12].

Phase identification in as-grown and annealed fibres has been performed through powder X-ray diffraction (XRD) analysis, at room temperature, using a Panalytical X'pert PRO3 (CuKα1 radiation) between 10 and 70 º. The percentage of each phase was determined from the XRD results using the RIR method. Microstructural studies were performed on longitudinal polished sections of samples in an SEM (Su-70, Hitachi) to determine the phases content and distribution. Moreover, energy dispersive spectrometry (EDS,

Bruker) has been used to qualitatively establish the phases composition. Electrical resistivity and Seebeck coefficient were simultaneously measured on all samples by the standard DC four-probe technique, using the steady-state mode, in an LSR-3 system (Linseis GmbH) between 50 and 800 ºC under He atmosphere. These measurements were performed along the growth direction of the fibre. These data have been subsequently used to calculate the power factor, which was used to compare the electrical performances of samples.

Thermal diffusivity (α) was measured in a commercial Linseis LFA system between 100 ºC and 950 ºC. The transversal section of samples was covered with a graphite screen to ensure full absorption of the flashlight at the front surface and obtain high emissivity from the backside. For each sample, several diffusivity measurements were performed under the same conditions to ensure the reproducibility of experimental results and assure that no changes in samples or damage of the graphite screen have been produced during the experiment. The thermal conductivity was determined using the expression $\kappa = \alpha \cdot Cp \cdot d$, where α is thermal diffusivity, d is the density obtained through the Archimedes method, and Cp is the specific heat calculated using Dulong-Petit law. Finally, with the power factor and thermal conductivity values, ZT has been calculated to determine the thermoelectric performances of the samples.

Results & Discussion

As-grown samples

Powder XRD patterns of the as-grown fibres are represented in Fig. 1. As it can be observed in the graph, all samples show similar diffraction peaks, where the major ones can be associated to the $Ca_{0.9}Gd_{0.1}MnO_3$ (indicated by ◆, XRD ICDD card 04-015-8452) thermoelectric phase. Moreover, $Ca_{1.7}Gd_{0.3}MnO_4$ (✱, XRD ICDD card 04-010-5374) and $CaMn_2O_4$ (●, XRD ICDD card 01-070-4889) secondary phases have been identified in higher content when the growth rate is increased. These results are in agreement with previously reported data on the $CaMnO_3$ [18].

From these diffraction patterns, the amount of each phase in the different samples has been calculated, and the results are displayed in Table 1. From these data, it is clear that none of the samples is single phase, as expected, due to the incongruent melting of this compound. On the other hand, the proportion of the different phases is slightly changing with the growth speed, except for the highest rate where a drastic modification is produced. These results illustrate the influence of the pulling rate on the crystallization kinetics, which is characteristic of the Laser Floating Zone method [11].

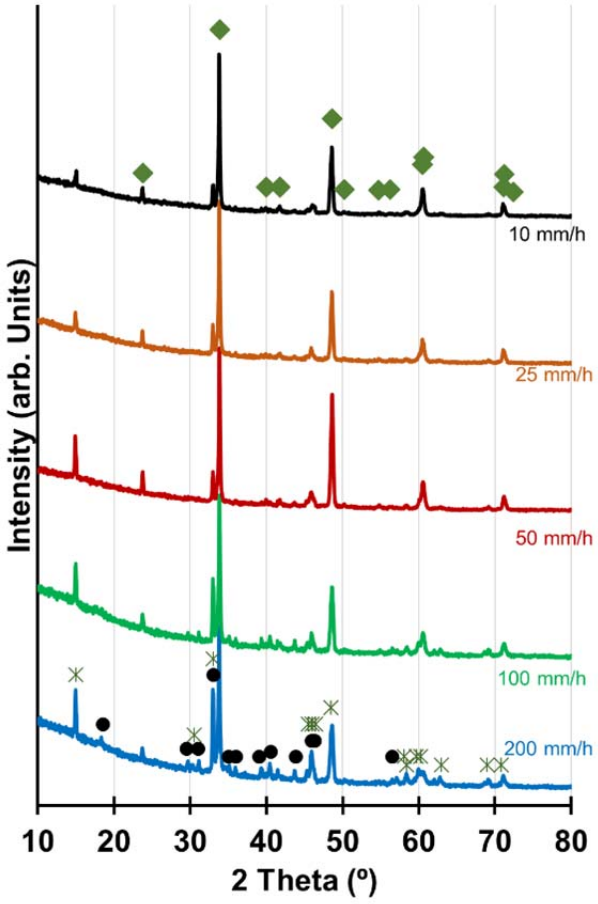

Figure 1. Powder XRD patterns of as-grown samples produced at different pulling rates. Peaks have been associated to different phases: $Ca_{0.9}Gd_{0.1}MnO_3$ (♦) thermoelectric phase; and $CaMn_2O_4$ (●), and $Ca_{1.7}Gd_{0.3}MnO_4$ (✱) secondary phases.

Table 1. Proportion of the different phases in as-grown fibres, as a function of the pulling rate.

Pulling rate (mm h^{-1})	$Ca_{0.9}Gd_{0.1}MnO_3$ Main Phase	$Ca_{1.7}Gd_{0.3}MnO_4$ Secondary Phase	$CaMn_2O_4$ Secondary Phase	Density (±0.02 g cm^{-3})
10	58	22	20	4.12
25	62	20	18	4.16
50	68	16	16	4.19
100	51	24	25	4.20
200	37	31	32	4.24

Microstructural observations performed on all samples have shown that they possess high density, and no porosity can be observed, in agreement with the density values present in table 1. Besides, an increase of density of the samples after LFZ growth, when compared to that of the seed (green bars, close to 1.34 g cm^{-3}), which is characteristic of the technique [11]. Moreover, they present good grain alignment along the growth direction, as illustrated in the representative micrographs displayed in Fig. 2. On the other hand, the different contrasts observed in these micrographs have been associated, through EDS analysis, to three different phases (see Fig. 2), which match with those identified through XRD, previously discussed. Furthermore, it can be also observed that the sizes of the secondary phases are decreasing when the pulling rate is reduced.

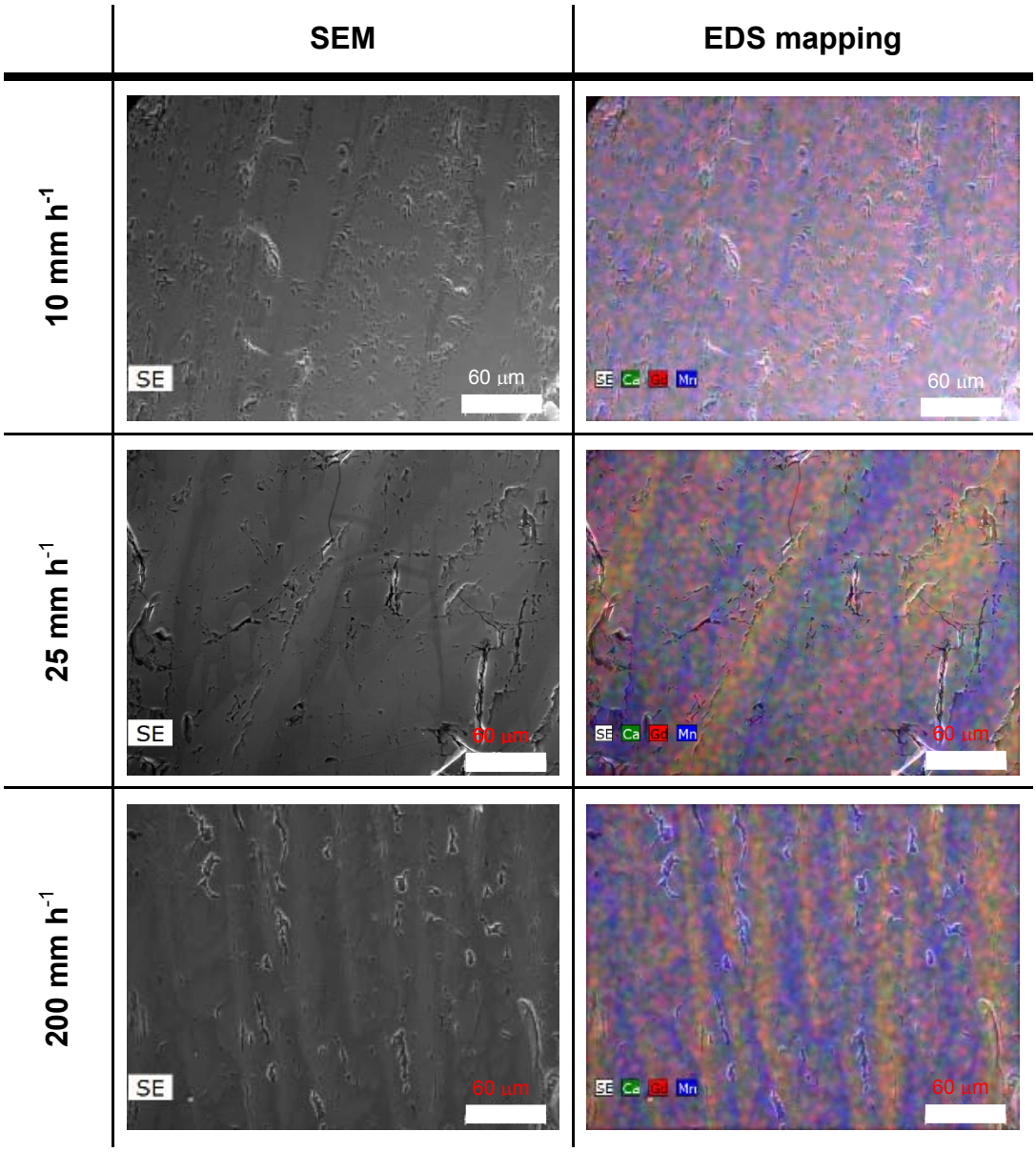

Figure 2. Representative SEM micrographs, and their corresponding EDS maps determined on polished longitudinal sections of as-grown samples at different pulling rates.

Electrical resistivity and Seebeck coefficient of as-grown fibres were not possible to be determined due to the very high electrical resistivity of samples which is out of the system measurement range. This fact shows that samples after the growth process do not display thermoelectric characteristics, not only due to the presence of secondary phases, but also to the presence of a high amount of oxygen vacancies in the thermoelectric phase, as previously reported for other thermoelectric ceramics [12,19]. As a consequence, taking into account previously reported results on materials grown through the laser

floating zone technique, such as $Ca_3Co_4O_9$, or bismuth [3] and $CaMnO_3$ [12] based materials, an annealing procedure can be useful to promote the formation of thermoelectric phase, and decrease the amount of oxygen vacancies. All these modifications should increase thermoelectric performances, as previously reported [3,12]. This annealing procedure consisted in an one.step heating at 1300 ºC for 10h under air, with a final furnace cooling to room temperature.

Annealed samples

After annealing, powder XRD results still show the presence of $Ca_{1.7}Gd_{0.3}MnO_4$ (XRD ICDD card 04-010-5374) and $CaMn_2O_4$ (XRD ICDD card 01-070-4889) secondary phases, while the $Ca_{0.9}Gd_{0.1}MnO_3$ (XRD ICDD card 04-015-8452) is the major one, with orthorhombic Pnma (62) structure The proportion of the different phases, has been determined and presented in Table 2, as a function of the growth rate. When compared to the results obtained in as-grown samples (see Table 1), the amount of the thermoelectric phase is largely increased after annealing treatment. This increase is due to the formation of the thermoelectric phase from the secondary ones at the annealing temperature, slightly rising, at the same time, samples density. Moreover, the amount of thermoelectric phase is further increased when the growth rate is decreased. On the other hand, a very slight decrease of samples density can be observed when the amount of thermoelectric phase increases, associated to lower growth rates (Table 2). This effect confirms the presence of higher content of secondary phases in the fibres grown at higher rates, and the evolution can be associated to the different densities of the secondary phases ($CaMn_2O_4$ = 3.94 g cm^{-3} [20] and $Ca_{1.7}Gd_{0.3}MnO_4$ above that, we can estimate above the density of Ca_2MnO_4 ~ 4.07 g cm^{-3} [21], when compared to the thermoelectric one ($Ca_{0.9}Gd_{0.1}MnO_3$ = 4.90 g cm^{-3}, XRD ICDD card 04-015-8452).

Table 2. Proportion of different phases in annealed fibres grown with different pulling rates.

Pulling rate (mm h^{-1})	$Ca_{0.9}Gd_{0.1}MnO_3$ Main Phase	$Ca_{1.7}Gd_{0.3}MnO_4$ Secondary Phase	$CaMn_2O_4$ Secondary Phase	Density (±0.02 g cm^{-3})
10@HT	**90**	**10**	**-**	**4.14 (84.5%)**
25@HT	**89**	**11**	**-**	**4.19 (85.5%)**
50@HT	**88**	**12**	**-**	**4.21 (85.9%)**
100@HT	**68**	**13**	**19**	**4.22 (86.1%)**
200@HT	**71**	**12**	**17**	**4.29 (87.6%)**

This phase evolution has also been corroborated through SEM observations and EDS analysis, as it can be observed in the representative images displayed in Fig. 3. In these images, it can be seen that there are three regions in all the samples, associated through EDS to different phases. Moreover, at low pulling rates (10 – 50 mm h^{-1}) a major phase, accompanied by small secondary phases, with a good grain orientation along the growth direction, can be observed. On the other hand, at higher growth rates, an increase of grain misorientation, with larger secondary phases, can be observed.

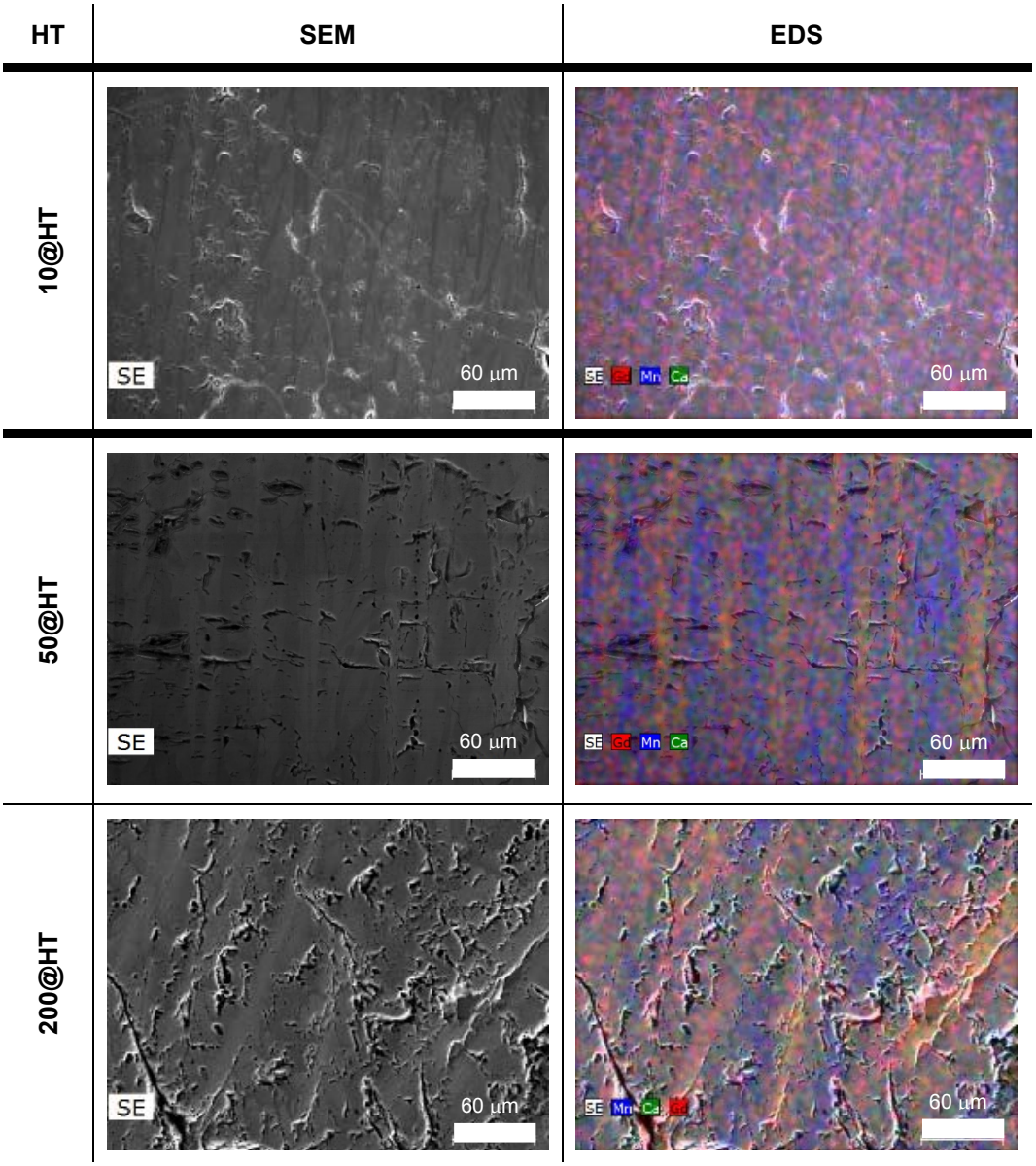

Figure 3. Representative SEM micrographs obtained on longitudinal cross-sections of samples grown at 10, 50, and 200 mm h^{-1}, together with their EDS elemental maps.

The decrease of secondary phases content, when the pulling rate is lower, significantly influences the electrical resistivity of the annealed samples, as shown in Fig. 4a. As it can be observed in the graph, all samples present semiconducting behaviour, except for the lowest growth rate samples, in the whole measured temperature range. This behaviour is different from the typical obtained in this family, which is metallic for sintered materials [3,4,10,22]. This difference clearly reflects the fact that as-grown samples possess very high density (Table 1) and, consequently, oxygen diffusion to the inner part of the

samples is hindered during annealing, even at high temperatures (Table 2). On the other hand, the electrical resistivity results illustrate the effect of growth rate, as lower rates lead to lower resistivity due to the decrease of secondary phases content, and better grain alignment. The lowest values determined at room temperature (~ 0.3 mΩ.cm) have been obtained in 10 mm h^{-1} grown fibres. These values are much lower than those measured in sintered $CaMnO_3$ (125 mΩ.cm) [23], spark plasma sintered (SPS) materials (10 mΩ.cm) [24], or even in $Ca_{0.9}Gd_{0.1}MnO_3$ + 5% K_2CO_3 used as a reference in the graph (4 mΩ.cm) [4]. Furthermore, they are much lower than the best reported results in doped or co-doped $CaMnO_3$ (2.3-100.0 mΩ.cm) [5,12,25-27].

Seebeck coefficient evolution with temperature for all samples is displayed in Fig. 4b. As it can be seen, all fibres exhibit negative values, indicating that the predominant charge carriers are electrons (n-type conduction). Moreover, absolute S values increase with temperature, which is the typical behaviour of the manganites family [3,5,11,28,29]. Besides, absolute S values tend to decrease when the growth rate is increased, that could be due to the decrease of the $Ca_{0.9}Gd_{0.1}MnO_3$ phase content. The highest values at room temperature (~ 75 μV K^{-1}) are lower than the reported for pure $CaMnO_3$ (-350 μV K^{-1}) [9], reflecting the higher carrier concentration in the doped materials. On the other hand, these values are in the same order of those reported in doped materials (between -50 and -400 μV K^{-1}) [5,11,12,24-27].

Electrical performances of the samples, determined through the power factor as a function of growth rate, has been calculated and it is presented in Fig 4c. As it can be observed in the graph, PF values tend to increase when the growth rate is decreased, in agreement with the lower electrical resistivity determined in these samples. The highest PF values at 800 °C (~0.35 mW m^{-1} K^{-2}) are within the data reported in the literature (Table 3), being similar to the optimally doped $CaMnO_3$ (0.34-0.4 mW m^{-1} K^{-2}) [11,27], but higher than the reported in the $CaGdMnO_3$ system (0.67-1.21 μW m^{-1} K^{-2} [5]), in $Ca_{0.9}Yb_{0.1}MnO_3$ (0.1-0.24 (mW m^{-1} K^{-2} [25]), or the $CaSrMnMoO_3$ system (0.05-0.25 (mW m^{-1} K^{-2} [30]).

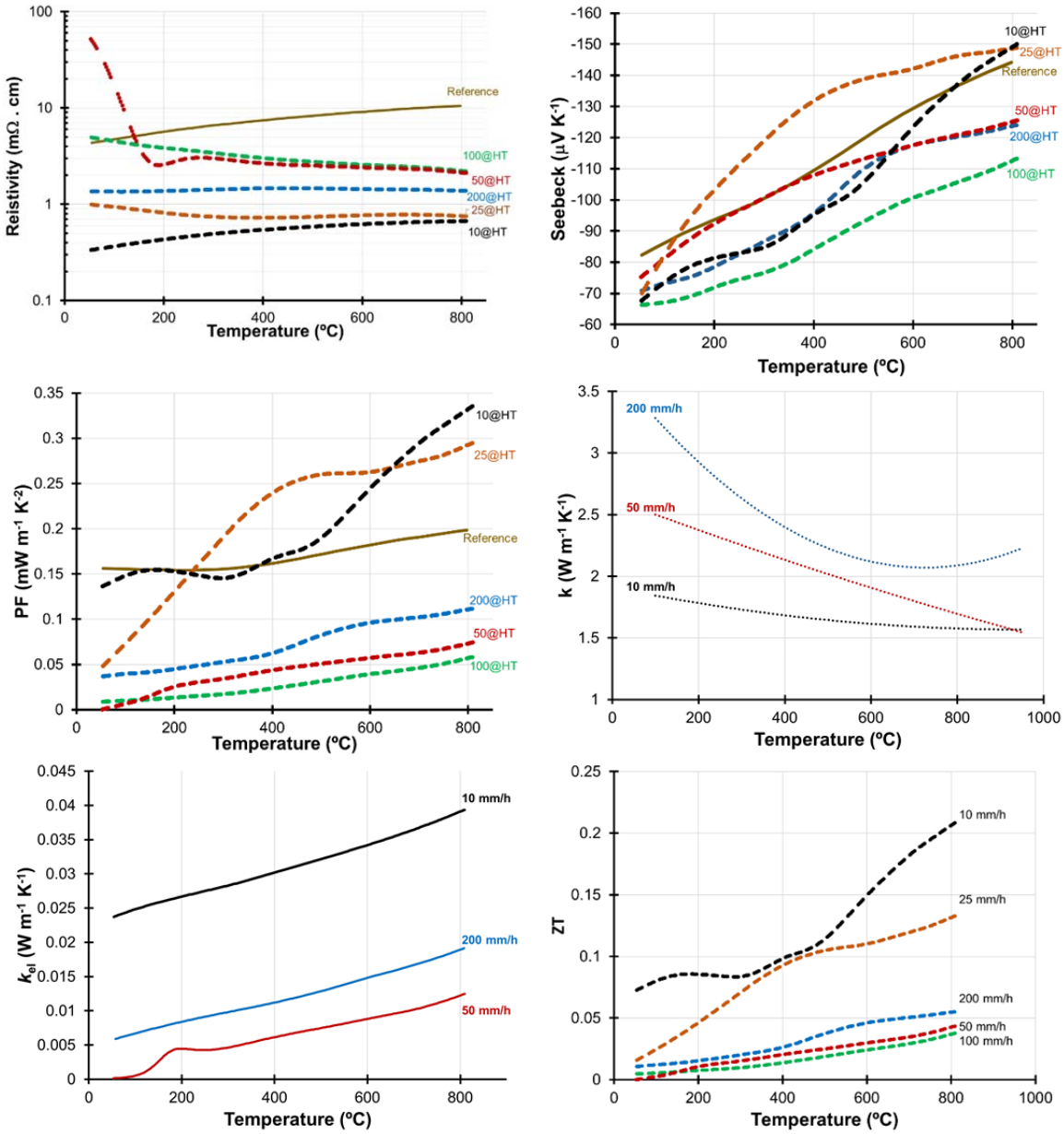

Figure 4. a) Electrical resistivity, b) Seebeck coefficient, c) Power Factor, d) thermal conductivity, e) electronic contribution of thermal conductivity, f) ZT evolution with temperature, for annealed samples grown at different pulling rates. Reference corresponds to the $Ca_{0.9}Gd_{0.1}MnO_3$ + 5% K_2CO_3 sample [4].

Total thermal conductivity (κ) can be expressed as:

$$\kappa = \kappa_{el} + \kappa_{ph},$$

where κ_{el} and κ_{ph} represent the electronic and lattice thermal conductivity, respectively. The electronic contribution (κ_{el}) can be calculated by using the Wiedemann-Franz-Lorenz relationship:

$$\kappa_{el} = \frac{L_0\, T}{\rho}$$

where L_0 = 2.45 × 10^{-8} W Ω K^{-2} is the Lorenz number, T the absolute temperature, and ρ the electrical resistivity [1].

Table 3. Comparison of PF (power factor), total thermal conductivity (k) and electronic thermal conductivity (k_{el}) values obtained in this work with those reported in the literature.

Systems	PF ($mWm^{-1}K^{-2}$)	K ($Wm^{-1}K^{-1}$)	Kel ($Wm^{-1}K^{-1}$)
$Ca_{0.9}Gd_{0.1}MnO_{3-\delta}$ by LFZ Present work	0,..,0.35	1.5,..,3.25	0.040-0.010
$Ca_{0.9}Gd_{0.1}MnO_{3-\delta}$ +K_2CO_3 [4]	0,…,0.56	0.64,..,1.22	0.036,..0.183
$Ca_{0.98\text{-}0.95}Gd_{0.02\text{-}0.05}MnO_{3-\delta}$ [5]	0.67,..,1.21	1.26,..,1.99	0.027
$CaMnO_{3-\delta}$ [5]	0.99	03.72	0.019
$Ca_{0.96}Gd_{0.04}MnO_{3-\delta}$ [18]	~0.3	2,..,4.75	0.030,..,0.089

The thermal conductivity evolution with temperature for all fibres is shown in Fig. 4d. As it can be observed, κ is in the 1.5 – 3.5 W m^{-1} K^{-1} range at room temperature, and decreases when the pulling rate is lower, indicating an influence of the grain alignment (texturization). Moreover, these values are decreased when the temperature is raised. The obtained values in this work are within the reported in previous work (Table 3). On the other hand, the electronic contribution of thermal conductivity (κ_{el}) presents the opposite behaviour with the pulling rate (Fig. 4e), these κ_{el} values are also within the data presented in the literature (Table 3). The decrease of κ_{el} can be ascribed to an increase of crystallographic distortion [5], which is produced, in this case, by the higher pulling rate. In any case, κ_{el} values are negligible when compared to the κ_{ph} contribution.

Using PF, and κ values, ZT has been calculated and displayed, as a function of temperature and growth rates, in Fig. 4f. In the graph, it is clear that the highest ZT values have been determined in samples grown at the lowest pulling rates. Nevertheless, these fibres present ZT close to the reported for the K-doped

$Ca_{0.9}Gd_{0.1}MnO_3$ samples (~ 0.22) prepared through the solid-state route [4]. Moreover, these values are within the range reported in the literature for $CaMnO_3$ based-system [5,10,28,29]. In spite of these close values, the samples prepared in this work show an additional advantage: these grown samples can be directly used to build thermoelectric modules with no additional machining. The best ZT values have been determined in samples grown at 10 mm h^{-1} associated to their low resistivity due to the presence of higher amount of thermoelectric phase. On the other hand, pulling rates above 50 mm h^{-1} lead to negligible differences between the samples. However, the samples grown at 50 mm h^{-1} present a transition between high and low pulling rates, that affects the electrical behaviour and phase distribution. These samples present a phases content very close to those grown at low pulling rates, while the electric behaviour is similar to those grown at high pulling rates. This result can be due to the lower grain orientation when compared to the samples grown at low rates, and the reduction of the $CaMn_2O_4$ phase content in these samples, when compared to those grown at high rates.

These results show that the annealing procedure of as-grown samples is very attractive for improving their thermoelectric properties, while keeping their useful geometry to build thermoelectric modules. Further efforts might be focused on the application of the proposed approach to other calcium manganites based materials with reasonable thermoelectric performances, with emphasis on the reduction of the secondary phases content, as already observed in p-type materials [31]. Moreover, these performances are accompanied, at the same time, by an adequate shape for a direct application as *n*-type leg to build high-temperature generation thermoelectric modules, avoiding further fabrication steps.

Conclusions

$Ca_{0.9}Gd_{0.1}MnO_3$ thermoelectric materials have been prepared through the Laser Floating Zone method using different pulling rates from 10 to 200 mm h^{-1}. XRD analysis showed the presence of perovskite-type phase as the major one in all samples. The amount of secondary $CaMn_2O_4$ and $Ca_3Mn_2O_7$ phases has been

significantly reduced by using slower pulling rates, as well as annealing these as-grown fibres. This annealing procedure allows measuring the thermoelectric performances of the fibres. A power factor of ~0.35 mW m^{-1} K^{-2} at 800 ºC, with thermal conductivity around 2 W m^{-1} K^{-1} was obtained for the lowest pulling rate. Thermal conductivity decreases when the temperature is increased due to a lower lattice contribution. ZT close to 0.22 was achieved for samples grown at the lowest pulling rate (10 mm h^{-1}) after annealing, being around the best-reported values in the literature. The results suggest that annealing as-grown fibres are very attractive for improving n-type materials for high-temperature thermoelectric applications, with the additional advantage of adequate dimensions for their direct use as n-type legs in thermoelectric modules.

Declaration of Interests

The authors declare no competing interests

Acknowledgements

The authors gratefully acknowledge the support of i3N (UID/CTM/50025/2019) and CICECO-Aveiro Institute of Materials (UID/CTM/50011/2019), financed by national funds through the FCT/MEC and when appropriate co-financed by FEDER under the PT2020 Partnership Agreement. This work is funded by national funds (OE), through FCT – Fundação para a Ciência e a Tecnologia, I.P., in the scope of the framework contract foreseen in the numbers 4, 5 and 6 of the article 23, of the Decree-Law 57/2016, of August 29, changed by Law 57/2017, of July 19.

M. A. Madre and A. Sotelo recognize the MINECO-FEDER (MAT2017-82183-C3-1-R) and Gobierno de Aragon-FEDER (Research Group T 54-17 R) for funding.

References

[1] S. Walia, S. Balendhran, H. Nili, S. Zhuiykov, G. Rosengarten, Q.H. Wang, M. Bhaskaran, S. Sriram, M.S. Strano, K. Kalantar-zadeh, Transition metal oxides – Thermoelectric properties, Progress in Materials Science 58 (2013) 1443–1489, DOI: 10.1016/j.pmatsci.2013.06.003.

[2] F.P. Zhang, Q.M. Lu, X. Zhang, J.X. Zhang, First principle investigation of electronic structure of CaMnO3 thermoelectric compound oxide, Journal of Alloys and Compounds 509 (2011) 542–545, DOI:10.1016/j.jallcom.2010.09.102.

[3] Sotelo A, Torres M, Madre M, Diez J. Effect of synthesis process on the densification, microstructure, and electrical properties of $Ca_{0.9}Yb_{0.1}MnO_3$ ceramics, Int J Appl Ceram Technol. 14 (2017) 1190–1196, DOI: 10.1111/ijac.12711.

[4] N. M. Ferreira, M. C. Ferro, A. R. Sarabando, A. Ribeiro, A. Davarpanah, V. Amaral, M. A. Madre, A. V. Kovalevsky, M. A. Torres, F. M. Costa, A. Sotelo, Improvement of thermoelectric properties of $Ca_{0.9}Gd_{0.1}MnO_3$ by powder engineering through K_2CO_3 additions, Journal of Materials Science 54 (2018) 3252–3261, DOI:10.1007/s10853-018-3058-x~.

[5] Ankam Bhaskar, Chia-Jyi Liu, and J. J. Yuan, Thermoelectric Properties of $Ca_{1-x}Gd_xMnO_{3-\delta}$ (0.00, 0.02, and 0.05) Systems, The Scientific World Journal Volume 2012, Article ID 149670, 5 pages, DOI:10.1100/2012/149670.

[6] M. Rosić, Lj. Kljajević, D. Jordanov, M. Stoiljković, V. Kusigerski, V. Spasojević, B. Matović, Effects of sintering on the structural, microstructural and magnetic properties of nanoparticle manganite $Ca_{1-x}Gd_xMnO_3$ (x=0.05; 0.1; 0.15; 0.2), Ceramics International, 41 (2015) 14964–14972, DOI: 10.1016/j.ceramint.2015.08.041.

[7] M. Ohtaki, H. Koga, T. Tokunaga, K. Eguchi, H. Arai Electrical transport properties and high-temperature thermoelectric performance of (Ca0.9M0.1) MnO3 (M = Y, La, Ce, Sm, In, Sn, Sb, Pb, Bi) J. Solid State Chem., 120 (1995), pp. 105-111

[8] G.J. Xu, R. Funahashi, I. Matsubara, M. Shikano, Y.Q. Zhou High-temperature thermoelectric properties of the Ca1−xBixMnO3 system J. Mater. Res., 17 (2002), pp. 1092-1095

[9] R. Kabir, R. Tian, Role of Bi doping in thermoelectric properties of $CaMnO_3$, Journal of Alloys and Compounds, 628 (2015) 347-351, DOI: 10.1016/j.jallcom.2014.12.141.

[10] H. Wang, W. Su, J. Liu, C. Wang (2016) Recent development of n-type perovskite thermoelectrics, J Materiomics 2, 225-236, DOI:10.1016/j.jmat.2016.06.005.

[11] N.M. Ferreira, N.R. Neves, M.C. Ferro, M.A. Torres, M.A. Madre, F.M. Costa, A. Sotelo, A.V. Kovalevsky (2019) Growth rate effects on the thermoelectric performance of $CaMnO_3$-based ceramics, J. Eur. Ceram. Soc. 39, 4184. DOI: 10.1016/j.jeurceramsoc.2019.06.011.

[12] F.P. Carreira, N.M. Ferreira, A.V. Kovalevsky, Laser processing as a tool for designing donor-substituted calcium manganite-based thermoelectrics, Journal of Alloys and Compounds 829 (2020) 154466, DOI: 10.1016/j.jallcom.2020.154466.

[13] Y. Wang, Y. Sui, High temperature thermoelectric response of electron-doped $CaMnO_3$, Chem. Mater. 21 (2009) 4653–4660, DOI: 10.1021/cm901766y.

[14] D. Enescu, Thermoelectric Energy Harvesting: Basic Principles and Applications, in Green Energy Advances edited by Diana Enescu, Published by Intechopen February 2019, ISBN: 978-1-78984-200-5, DOI: 10.5772/intechopen.83495

[15] Poudel B., Hao Q., Ma Y., Lan Y., Minnich A., Yu B., Yan X., Wang D., Muto A., Vashaee D., Chen X., Liu J., Dresselhaus M.S., Chen G., Ren Z. (2008) High-thermoelectric performance of nanostructured bismuth antimony telluride bulk alloys. Science 320, 634-638.

[16] F. Giovannelli, C. Chen, P. Diaz-Chao, E. Guilmeau, F. Delorme (2018) Thermal conductivity and stability of Al-doped ZnO nanostructured ceramics. J. Eur. Ceram. Soc. 38, 5015-5020.

[17] Wang et al. enhanced thermoelectric performance of Nb-doped SrTiO3 by nano-inclusion with low thermal conductivity - scientific reports 3 (2013) 03449.

[18] R. Löhnert, M. JörgTöpfer, Evaluation of soft chemistry methods to synthesize Gd-doped $CaMnO_{3-\delta}$ with improved thermoelectric properties, Materials Science and Engineering: B, 223 (2017) 185-193, DOI: 10.1016/j.mseb.2017.06.014.

[19] Sh. Rasekh, M.A. Madre, A. Sotelo, E. Guilmeau, S. Marinel, J.C.Diez, Effect of synthetic methods on the thermoelectrical properties of textured $Bi_2Ca_2Co_{1.7}O_x$ ceramics, Bol. Soc. Esp. Ceram. V. 49, 1, 89-94 (2010).

[20] https://materialsproject.org/materials/mp-1004038/, last access Dec2019

[21] Pierre Villars, Ca2MnO4 Crystal Structure in: Inorganic Solid Phases, SpringerMaterials (online database), Springer, Heidelberg (ed.), https://materials.springer.com/isp/crystallographic/docs/sd_1102735, Heidelberg, © 2016), last access Aug2020

[22] M. Mouyane, B. Itaalit, J. Bernard, D. Houivet, J. G. Noudem, Flash combustion synthesis of electron doped-$CaMnO_3$ thermoelectric oxides, Powder Technology 264 (2014) 71–77, DOI: 10.1016/j.powtec.2014.05.022.

[23] J.G. Noudem, D. Kenfaui, S. Quetel-Weben, C.S. Sanmathi, R. Retoux, M. Gomina, Spark Plasma Sintering of n-Type Thermoelectric $Ca_{0.95}Sm_{0.05}MnO_3$, J Amer Ceram Soc.94 (2011) 2608-2612, DOI: 10.1111/j.1551-2916.2011.04465.x.

[24] S. Quetel-Weben, R. Retoux, J.G. Noudem, Thermoelectric $Ca_{0.9}Yb_{0.1}MnO_{3-\delta}$ grain growth controlled by spark plasma sintering, J Eur Ceram Soc. 33 (2013) 1755-1762, DOI: 10.1016/j.jeurceramsoc.2013.02.003.

[25] R. Kabir, D. Wang, T. Zhang, R. Tian, R. Donelson, T.T. Tan, S. Li, Tunable thermoelectric properties of $Ca_{0.9}Yb_{0.1}MnO_3$ through controlling the particle size via ball mill processing, Ceram Int. 40 (2014) 16701-16706, DOI: 10.1016/j.ceramint.2014.08.033.

[26] H. Wang, C. Wang, Synthesis of Dy doped $Yb_{0.1}Ca_{0.9}MnO_3$ ceramics with a high relative density and their thermoelectric properties, Mater Res Bull. 47 (2012) 2252-2256, DOI: 10.1016/j.materresbull.2012.05.061.

[27] Y. Zhu, C. Wang, H. Wang, W. Su, J. Liu, J. Li, Influence of Dy/Bi dual doping on thermoelectric performance of $CaMnO_3$ ceramics, Mater Chem Phys. 144 (2014) 385-389, DOI: 10.1016/j.matchemphys.2014.01.006.

[28] J.W. Park, D.H. Kwak, S.H. Yoon, S.C. Choi, Thermoelectric properties of Bi, Nb co-substituted $CaMnO_3$ at high temperature, Journal of Alloys and Compounds 487 (2009) 550–555, DOI:10.1016/j.jallcom.2009.08.012.

[29] M. Molinari, D. A. Tompsett, S. C. Parker, F. Azoughb, R. Freerb, Structural, electronic and thermoelectric behaviour of $CaMnO_3$ and $CaMnO_{(3-\delta)}$, J. Mater. Chem. A 2 (2014) 14109, DOI: 10.1039/c4ta01514b.

[30] D. Srivastava, F. Azough, R. Freer, E. Combe, R. Funahashi, D. M. Kepaptsoglou, Q. M. Ramasse, M. Molinari, S.R. Yeandel, J.D. Barand, S.C. Parker, Crystal structure and thermoelectric properties of Sr–Mo substituted $CaMnO_3$: a combined experimental and computational study, J. Mater. Chem. C, 3 (2015) 12245, DOI: 10.1039/c5tc02318a.

[31] G. Constantinescu, Sh. Rasekh, M.A. Torres, J.C. Diez, M.A. Madre, A. Sotelo, Effect of Sr substitution for Ca on the $Ca_3Co_4O_9$ thermoelectric properties, J. Alloys Compd. 577 (2013) 511–515, DOI: 10.1016/j.jallcom.2013.07.005.